Preprints.org

Article

Not peer-reviewed version

Stitch-Less Lithography Empowered by Multi-Dimensional Holography

Hsin-Hui Huang * , Haoran Mu , Eulalia Puig Vilardell , Vijayakumar Anand , Darius Gailevičius , Saulius Juodkazis *

Posted Date: 15 May 2026

doi: 10.20944/preprints202605.1037.v1

Keywords: stitching-less lithography; resolution; feature size; threshold effect; diffraction limit; microfabrication; 3D

Preprints.org is a free multidisciplinary platform providing preprint service that is dedicated to making early versions of research outputs permanently available and citable. Preprints posted at Preprints.org appear in Web of Science, Crossref, Google Scholar, Scilit, Europe PMC, OpenAlex.

Copyright: This open access article is published under a Creative Commons CC BY 4.0 license, which permit the free download, distribution, and reuse, provided that the author and preprint are cited in any reuse.

Preprints.org (www.preprints.org) | NOT PEER-REVIEWED | Posted: 15 May 2026 doi:10.20944/preprints202605.1037.v1

Disclaimer/Publisher's Note: The statements, opinions, and data contained in all publications are solely those of the individual author(s) and contributor(s) and not of MDPI and/or the editor(s). MDPI and/or the editor(s) disclaim responsibility for any injury to people or property resulting from any ideas, methods, instructions, or products referred to in the content.

Article

Stitch-Less Lithography Empowered by Multi-Dimensional Holography

Hsin-Hui Huang [1,2,3,*], Haoran Mu [1,3], Eulalia Puig Vilardell [4,5], Vijayakumar Anand [1], Darius Gailevičius [4], Saulius Juodkazis [1,4,6,*]

[1] Optical Sciences Centre, Swinburne University of Technology, Hawthorn, Victoria 3122, Australia
[2] Australian Research Council (ARC) Industrial Transformation Training Centre in Surface Engineering for Advanced Materials (SEAM), Swinburne University of Technology, Hawthorn, VIC, 3122, Australia
[3] Melbourne centre for Nanofabrication (MCN), 151 Wellington Road, Clayton, Vic 3168, Australia
[4] Laser Research Center, Physics Faculty, Vilnius University, Saulėtekio Ave. 10, 10223 Vilnius, Lithuania
[5] Institute of Physics, University of Tartu, W. Ostwaldi 1, 50411 Tartu, Estonia
[6] World Research Hub (WRH), School of Materials and Chemical Technology, Institute of Science Tokyo, 2-12-1, Ookayama, Meguro-ku, Tokyo 152-8550, Japan
* Correspondence: hsinhuihuang@swin.edu.au (H.-H.H.); sjuodkazis@swin.edu.au (S.J.)

Abstract

Trends in Micro- and Nano-Lithography required for future development of large area applications ranging from high-packing-density electronics to solar cells are surveyed and outlined. Strategies to use direct laser writing to define etch masks over large areas by: i) fixed beam moving stage and ii) moving beam moving stage approaches are presented. The extension of planar 2D and stacked 2D (or 2.5D) fabrication methods into 3D micro- and nano-fabrication is discussed. One of the essential future characteristic of 3D nanolithography is real-time feedback capability. This can be realised via inherent 3D-capable holography, which bridges lithographic exposure control, wavefront sensing, and adaptive feedback, providing a pathway to stitch free, large area 3D patterning. The future of micro-fabrication is expected to evolve via highly specialised 3D architecture design and reduction of post-processing steps.

Keywords: stitching-less lithography; resolution; feature size; threshold effect; diffraction limit; microfabrication; 3D

1. E/O-Moore's Laws

The (electronics) e-Moore's law of transistor number doubling every two years [1–3], which is based on the development of planar two-dimensional (2D) nanolithography (Figure 1), is the driving force for the growth of the closely interconnected fields of computers, telecommunications, fibre-optics, mobile phones, and, more recently, artificial intelligence (AI). The (optical) o-Moore's law shows the same tendency of doubling the number of photons every two years (and hence average laser power) for ultra-short pulsed lasers [4–6]. This tendency is clear only for the past 25 years [7]. Arguably, it is driven by new applications of ultra-short laser machining [8,9], which match the challenge for higher average power requirements by the advancement of laser sources when more power is extracted from the excited crystal in the cavity [10–13].

The fundamental difference between the two laws, e-Moore's and o-Moore's laws, is that the latter powers applications of direct laser write and sequential material processing (machining) [4,14], while e-Moore's law's success is due to its parallel-processing nature. In this perspective, promising approaches for the development of large-area direct write applications are overviewed, with arguments presented for when direct write (sequential mode) could challenge parallel-mode lithography. In these areas of technology development, the potential for real industrial application is greatest. Now is the right time to ask questions about promising directions and anticipate the most efficient uptake of laser technologies. This tension between sequential and parallel approaches is not only technical, but also

© 2026 by the author(s). Distributed under a Creative Commons CC BY license.

reflects a broader industrial logic: performance leads, cost follows. This is the "Better Before Cheaper" principle at the global trend of the "fusion-era" (Figure 2).

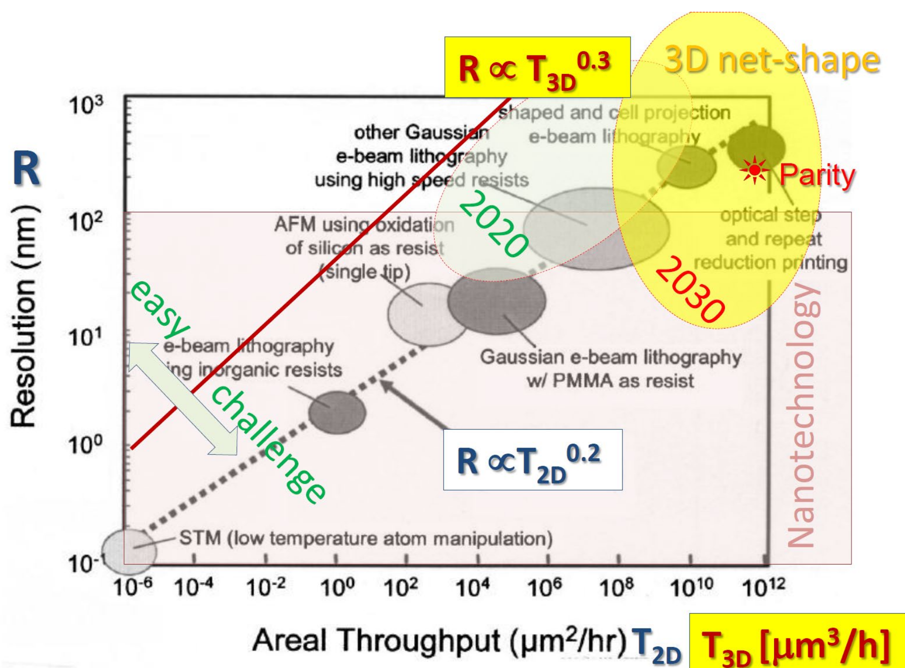

Figure 1. Our established 3D printing dependence of resolution R vs throughput T_{3D} is based on Tennant's scaling [15], to be further facilitated by the Moore's law for average power fs-laser we revealed [4]. The recent (2020) and future (2030) throughput and resolution capability ranges are shown. Conventional electrical discharge machining (EDM) achieves 3 mm^3/min material removal rate. The Parity point using fs-laser fabrication was reached in 2016 [16], when the material removal rate by laser and by current spark(mechanical)-machining become equal. Mesoscale resolution from nm-to-mm is the aim based on high-energy density fabrication.

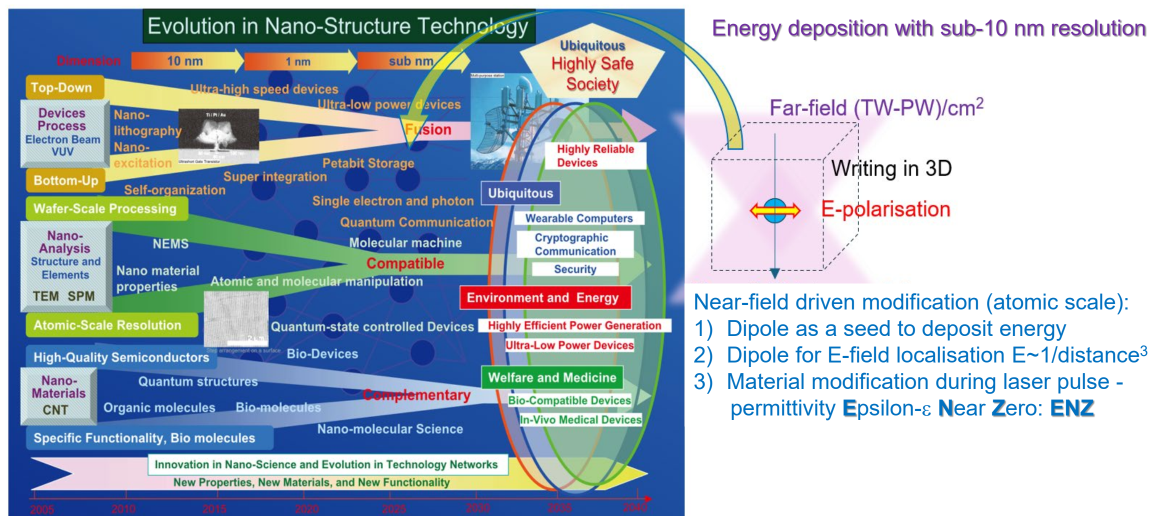

Figure 2. The "fusion era" of previously exclusive approaches is expected to start from 2025 onward. This roadmap, developed by the Japan Society of Applied Physics (JSAP) - a leading knowledge economy - strategically addresses societal needs [17]. The right-side inset shows dipole nano-seed as a 2D/3D laser writing tool. The intensity of dipole source is localised as $I \propto r^6$, where r is polar coordinate (radius of point-like energy deposition). The most efficient energy deposition is near the dielectric breakdown, which is defined when permittivity $\varepsilon = n^2 - \kappa^2 = 0$ defined by the complex refractive index $\tilde{n} = n + i\kappa$. This is the ENZ state of material.

Preprints.org (www.preprints.org) | NOT PEER-REVIEWED | Posted: 15 May 2026 doi:10.20944/preprints202605.1037.v1
© 2026 by the author(s). Distributed under a Creative Commons CC BY license.

Preprints.org (www.preprints.org) | NOT PEER-REVIEWED | Posted: 15 May 2026 doi:10.20944/preprints202605.1037.v1

2. BBC - Better Before Cheaper

The motivation for this perspective is to identify which emerging fabrication technologies can deliver meaningful gains in performance and functionality, based on their technical simplicity or complexity, flexibility across different material systems, ability to operate over wide spatial and temporal scales, and overall technological maturity.

Direct laser writing and machining, compared to extreme ultraviolet (EUV), X-ray, e-beam, or ion-beam tools, have historically been adopted first in application domains where flexibility, rapid iteration, and material compatibility outweigh pure throughput. This dynamic reflects a broader "Better Before Cheaper" (BBC) principle [18]. It refers to the observation that higher margins from differentiation contribute more to the return on investment than efficiency gains from cost leadership [19]. In the current context, this relates to device architectures, substrates, and functional requirements that evolve rapidly; performance and adaptability must advance before cost or large-scale productivity becomes decisive. A decade ago, ultrashort-pulse laser fabrication had already enabled optical memories with densities beyond 1 Tbit/cm^3, waveguide-based optical information processing structures, 3D photonic crystals, micro-mechanical devices, and components for optical quantum systems [15,20–23]. These achievements underscored that early adoption was driven by function-first demand: researchers needed access to programmable, maskless, three-dimensional fabrication long before parallel lithography infrastructures could accommodate such geometries.

Today, in 2026, this trajectory has widened considerably, with applications ranging from high-packing-density electronics to solar cells increasingly relying on heterogeneous material stacks, extended substrate sizes, and device architectures that combine nanometre-scale features with micrometre- to millimetre-scale structures [24,25]. These emerging domains—including 3D integrated photonics, metasurface-encoded optics, quantum photonics, and microfluidic–opto-mechanical systems—require fabrication strategies capable of tolerating material diversity and supporting rapid design variation within a single multi-scale workflow [15,26–30]. In this context, lithographic strategies that emphasise flexibility, programmability, and multi-scale capability become particularly attractive. Examples illustrating how the flexibility of direct-writing approaches spans from fundamental material limits to full device-scale architectures can be found across diverse material platforms and applications. In the domain of 2D materials, which have emerged as an especially powerful platform for miniaturised optoelectronic and photonic devices, direct laser writing (via femtosecond laser scanning or scribing) has demonstrated angstrom-level removal depths and single-layer precision. This capability enables the thinning of graphene films to specific layer counts [31], as well as the fabrication of ultra-thin flat lenses through precise patterning of transition-metal dichalcogenides (TMDs) [32]. Moving from the control of vertical layer thickness to the pursuit of lateral resolution, direct super-resolution writing on GaAs has achieved lateral feature sizes as small as 32 nm, approximately one-tenth the diameter of the focused laser spot [33]. This was realised by selectively utilising the central region of the laser spot that exceeds the ablation threshold, enabling the fabrication of periodic nanostructures such as gratings and nano-holes. Such precision is essential for site-controlled quantum-dot growth and high-performance anti-reflection coatings. Resist free femtosecond laser patterning of graphene, MoS_2, and $PtSe_2$ has been demonstrated with sub-100 nm features using a commercial two-photon printer clearing a 200 μm $\times$ 200 μm area under 3 s [34]. On the opposite scale, direct write inside bulk glass has produced millimetre-scale plasmonic nanostructure arrays via near-field interaction, yielding structural colour and linear dichroism responses buried within the glass [35]. Together, these examples demonstrate that direct-writing techniques enable fabrication from the atomic-layer level to the architectural scales relevant for next-generation quantum and optoelectronic technologies.

Manufacturing has traditionally progressed in 7–10-year renovation cycles, prioritising reliability, tool longevity, and return on capital investment [15]. However, the industrial landscape has shifted: 3D device architectures, backside routing, advanced packaging, and yield-driven design now dominate lithographic requirements [24]. While resolution remains essential (Figure 3), system performance increasingly depends on depth-of-focus, overlay stability across warped or large substrates, and sup-

© 2026 by the author(s). Distributed under a Creative Commons CC BY license.

pression of stochastic patterning errors such as line edge roughness (LER), or partially stochastic such as edge placement error (EPE) and critical dimension uniformity (CDU) [24]. Packaging lithography in particular demands a large depth of field (DOF) and precise alignment on non-flat surfaces, conditions for which mask-based projection tools are not inherently optimised [24]. These realities reinforce the BBC logic: industrial scaling now values precision, adaptiveness, and local correction as highly as raw throughput. Direct writing, being maskless and reconfigurable at the level of individual features, is uniquely positioned to supply "better" fabrication capabilities before high-volume processes can catch up.

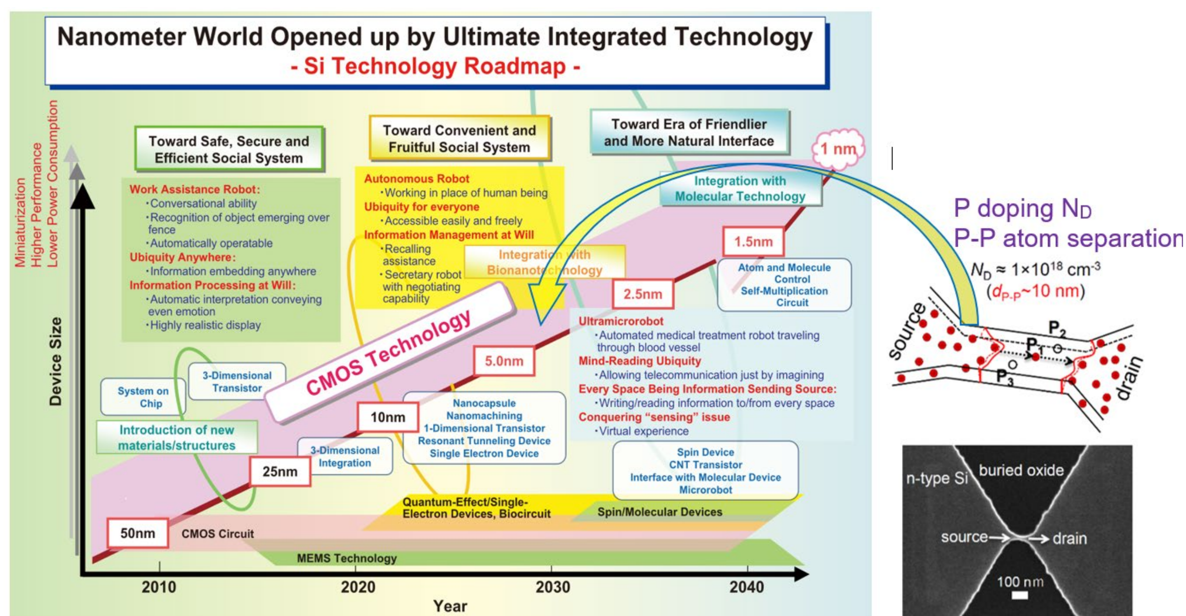

Figure 3. The potential of Si due to established CMOS technology [17]. A Si based CMOS-compatible approach for laser patterning of silicon to enable hyper-doping will allow single electron transistors (SETs) to operate at room conditions. The Si solar cell technology will surpass the current ray-optics Lambertian light trapping limit using large-area ~ 1 m^2 sub-micrometre patterning via femtosecond laser direct writing. The right-side inset illustrates an SET where a p-dopant atom (a quantum dot) controls the drain current. Hyper-doping at a concentration of 10^{20} cm^{-3} is required and could be achieved by fs-pulse triggered micro-explosion. At 10^{18} cm^{-3}, p-to-p dopant separation is ~ 10 nm; courtesy of Prof. D. Moraru.

This shift is supported by substantial technical advances in fs-laser fabrication. New generations of reliable MHz-to-GHz-class ultrafast sources, improved control of sub-100 nm feature sizes, and multi-NA mesoscale strategies (MBMS) enable structures spanning up to five orders of magnitude in scale [15]. Meanwhile, the broader lithography landscape, such as optical, EUV, e-beam, X-ray, and ion beam, shows clearer separation of strengths and limits [36]. Optical lithography remains diffraction-constrained and mask-dependent; EUV faces challenges related to LER, stochastic defects, resist chemistry, mask contamination, and high-vacuum infrastructure; e-beam maintains the finest resolution but remains throughput-limited; X-ray and ion-beam techniques use shorter wavelengths but carry burdens of mask deformation, vacuum requirements, or substrate damage [36].

Direct laser writing complements these methods by offering rapid prototyping, geometry freedom, and material diversity, often used to validate architectures before transferring stable parts of the flow to cheaper, higher-throughput projection lithography. The easiest way to imagine it is to consider master template fabrication using direct laser writing for nanoimprint lithography (NIL) [37,38]. Recent demonstrations prominently feature this BBC-workflow, in which complex micro-optics [39], photonic resonators [40,41], and plasmonic waveguides [42] are initially mastered via multiphoton lithography

Preprints.org (www.preprints.org) | NOT PEER-REVIEWED | Posted: 15 May 2026 doi:10.20944/preprints202605.1037.v1

© 2026 by the author(s). Distributed under a Creative Commons CC BY license.

Preprints.org (www.preprints.org) | NOT PEER-REVIEWED | Posted: 15 May 2026 doi:10.20944/preprints202605.1037.v1

and subsequently scaled for mass production via soft NIL [37]. It provided a rapid model-to-prototype pathway [43,44].

The emergence of 3D devices, backside metallisation, and chiplet-based integration requires fabrication strategies that provide localised precision, adaptive overlay control, and high depth-of-focus performance on non-planar or heterogeneous substrates [24]. These architectures intensify the demand for maskless, feedback-enabled direct writing, especially in stitching-critical or multi-material regions where traditional projection lithography struggles. Advanced packaging adds further constraints, as large substrates require a high DOF and tight overlay, while exposure methods that provide both high DOF and small pitches tend to be slow and expensive [24]. When combined with computational imaging and holography, femtosecond-laser-based direct writing can maintain accuracy over large areas, compensate for local topography, and suppress stochastic variations during fabrication. In this sense, BBC becomes a practical deployment strategy: rely first on methods that provide superior control and flexibility, then transition defined modules into high-throughput or lower-cost technologies once design and material specifications stabilise.

3. Stitching

One of the major challenges in large-area lithography is compensating for and reducing stitching errors when high-precision write fields must be seamlessly connected [45,46]. Another challenge is making high-resolution lithography masks (transmission or reflection) using electron beam lithography (EBL) [47,48]. Since such masks are made once and used for multiple (parallel) exposures, the efficiency of the approach is not bottlenecked [49]. For direct laser write (sequential) lithography, the bottleneck in producing the final pattern has to be addressed [50].

In EBL, the fixed beam moving stage (FBMS) was introduced, where a simple raster scan on a small scale is controlled by e-beam optics while e-resist is exposed on the substrate by moving the stage [51]. Raith EBL showed 10-nm-wide and 10-cm-long lines defined in the mask by EBL [52]. This technology was essential to progress in the last decade (or two) for micro-electronics due to the larger flexibility of available patterning compared with more specialised and faster pattern projection EBL tools [52,53]. This "democratisation" of EBL tools (also less capital investment) is well aligned with the popularity of 3D printing, which started as a pure prototyping method but has become a driving force in 3D fabrication in a very broad range of fields. The popularity of 3D printing is also based on the low cost of capital investment required, as well as the flexibility to change patterns and materials. It is noteworthy that recent direct write laser lithography tools based on laser diodes, e.g. PICOMASTER series, Raith, continue on stitch-less FBMS paradigm and can combine regions patterned at different resolutions $R \propto 1/NA$ by choice of objective lens with different numerical aperture NA.

In 3D laser lithography by direct writing, patterning areas larger than the available exposure or writing field of the tool was initially accomplished by separating the target layout into segments, sequentially writing and merging them into a continuous pattern [54]. Because adjacent fields must be precisely aligned and overlapped at their boundaries, any positional or geometric discrepancy in the stage or optical/scanning motion results in discontinuities, commonly termed stitching errors [54]. Stitching errors are therefore an intrinsic consequence of large-area patterning using mosaicked writing fields, which must be minimised to maintain pattern fidelity and device performance [55,56]. In practice, both minimisation and compensation strategies are used to address them [50]. A more flexible system that FBMS developed for EBL was made for 3D laser writing, which can be called moving beam moving stage (MBMS) [57]. This MBMS 3D laser printing is demonstrated with different parts of the structure with resolution and feature sizes from ~ 0.1 μm to ~ 10 mm, hence, spanning five orders of magnitude at the mesoscale [57]. This is achieved by a change of the numerical aperture NA of focusing optics as well as pulse energy and dose (via a scanning protocol) [55,58]. Changing the objective lens along the same optical axis does not change the lateral focal position by more than $(\lambda/NA)/20$, which is suitable for most demanding optical applications [59].

© 2026 by the author(s). Distributed under a Creative Commons CC BY license.

Lithographic definition of large masks over areas with cross sections tens-of-cm is another challenge relevant to stitching errors as well as for mask adhesion to the substrate. Plasma etching is preferable to wet etching using masks for defining nano-sized 3D surface structures, since capillary forces during rinsing and drying of the fabricated structures can induce mechanical failure and adhesion [60]. Critical point drying (CPD) is not always available/applicable and is an additional complication of technological processes. Plasma etching has another virtue, it preserves the designed pattern even in the case of under-cut etch (wet etching can damage the pattern once under-cut etch occurs below the mask) [61,62]. The downside of plasma etch is the affected semiconductor surface with tens-of-nanometres into sub-surface region and passivation by wet or dry processing should be applied after the etch [63,64].

For large area etch mask definition by lithography down to sub-micrometre structures, fs-laser direct write in tens-of-nm of alumina Al_2O_3 was proposed [65]. Ablation of dielectric nano-film opens a 200-300 nm hole for plasma etch [66]. Plasma etching removes the laser-affected region and forms an etched pit in the semiconductor/substrate [65,67]. The pattern of surface micro-pits for light trapping on the surface of a solar cell was made by this method [68]. This technology allows interference to be harnessed and can lead to 30% efficient Si solar cells and surpass the Lambertian light trapping limit all modern solar cells have as the limit [67,69]. By intentionally introducing non-ablated sites into a large area pattern [68], the mask area is defined and can withstand under-cut etch. This method of mask definition is compatible with the MBMS approach and can be scalable up to solar panel areas of ~ 1 m^2 [66]. One more advantage of direct write on large areas is the possibility to track the surface in real time, while the projection of a large mask in parallel lithography mode is more sensitive to good planar alignment [59,70].

Mitigation of stitching errors, whether through MBMS writing, adaptive stitching algorithms, or holographic parallel exposure, addresses only the planar, 2D dimension of the control problem. The deeper challenge is that femtosecond direct write is not a planar process: it creates three-dimensional (3D) distributions of modified material states inside a volume, and tracking, characterising, and correcting that volume in real time requires a fundamentally different approach.

4. 3D Challenge

The integration of multilayered electronic chips, optical interconnects, and 3D connector lines increasingly requires fabrication methods that can operate inside complex opto-electronic assemblies rather than only on planar surfaces (see roadmaps in Figures 2 and 3). Ultra-short-pulse laser machining is well suited to this task because it can deliver highly localised energy deposition with minimal mechanical contact and can, in principle, access buried or non-planar regions. The central difficulty, however, is no longer only how to write a pattern, but how to navigate and control the laser-material interaction in three dimensions.

In conventional planar lithography, the lateral position is usually constrained by stage encoders, scanner calibration, or interferometric positioning. By contrast, the axial coordinate, usually denoted as Z, is more difficult to stabilise because the focusing optics must remain suspended above the sample while the surface may be curved, tilted, thermally drifting, or optically heterogeneous. For delicate, transparent, multilayered, or partially processed substrates, contact-based height sensing is generally unsuitable; therefore, real-time optical focus tracking becomes essential. The practical requirement is stringent: the system must determine the position of the focal volume with minimal latency, preferably at nanoscale precision, while the sample and the written structure evolve during processing.

Several optical autofocus strategies have been developed for this purpose, including astigmatic focus-error detection, confocal reflectometry, and low-coherence interferometric sensing. Astigmatic detection is one of the most widely deployed focus-error sensing architectures [71–74]. In this method, the reflected tracking beam passes through a cylindrical lens before reaching a quadrant photodiode, so that axial displacement is converted into a change in the ellipticity and orientation of the detected spot [71,75]. Its main advantage is speed: the focus-error signal can be generated with little or no

© 2026 by the author(s). Distributed under a Creative Commons CC BY license.

Preprints.org (www.preprints.org) | NOT PEER-REVIEWED | Posted: 15 May 2026 doi:10.20944/preprints202605.1037.v1

computational delay, making the method attractive for high-bandwidth surface tracking [75]. Its limitation is that the signal is sensitive to sample tilt, local reflectivity, diffraction from patterned surfaces, and parasitic reflections from transparent layers [72,75–78].

Confocal methods provide a more selective axial response and are therefore useful for structured, reflective, or multilayered substrates [79–81]. They rely on spatial filtering: light from the focal plane is transmitted through a pinhole or equivalent detection aperture, while out-of-focus light is strongly rejected [82–84]. By detecting the axial position of maximum returned intensity, the system identifies the best focus [85,86]. The trade-off is that many confocal implementations require axial scanning, source modulation, or objective dithering to locate the peak, which introduces latency relative to purely astigmatic detection [86,87].

When absolute distance measurement, transparent-layer metrology, or robust operation over difficult topographies is required, low-coherence interferometry becomes the most powerful option [88–90]. These systems use broadband or swept-source illumination to compare the optical path length from the sample with that from a reference arm [89,91–93]. Interference occurs only when the optical paths match within the coherence length, allowing absolute surface position, optical thickness, or interface location to be extracted from the fringe signal [88,91–94]. This provides a more quantitative Z reference than relative focus-error methods and can be less sensitive to moderate changes in reflectivity or tilt [88,90,95]. However, real-time processing of interferometric spectra during high-speed transverse scanning requires specialised hardware, such as FPGA- or GPU-based reconstruction, and the optical architecture is correspondingly more complex and expensive [90,92,96,97].

These autofocus and distance-sensing methods address an essential but incomplete part of the 3D fabrication problem. They can stabilise the position of the focal volume relative to a surface or interface, but they do not by themselves identify the material state created inside the written voxel. This distinction becomes critical in modern femtosecond direct writing, where the laser does not merely define morphology but can also transform local optical, electrical, chemical, structural, and ferroic properties. A written voxel may therefore be multi-featured, it can possess a modified refractive index [98], birefringence [99], conductivity [100], crystallinity [101], defect density [102], oxidation state[103], stress field [104], or nanoscale phase composition [105]. The most striking property changes include the conversion of transparent diamond into conductive graphitic or graphenic networks [106,107], laser-induced amorphous-to-crystalline transitions [108], photo-response modification in patterned 2D materials [109], direct formation of oxygen-vacancy-rich metal-oxide semiconductors [110], and ultrafast synthesis of correlated metal-oxide transition materials [14].

This multi-property character of the written voxel has direct consequences for stitching. In conventional lithography, stitching error is treated as a positional problem: a misalignment of geometric boundaries between adjacent write fields. In femtosecond direct-write, misalignment of the addressable fields can also cause discontinuities in refractive index, birefringence, stress, or crystallinity at the stitch boundary, degrading the device's optical, electrical, or mechanical performance even when geometric alignment is achieved. A stitching strategy that achieves spatial continuity but not material-state continuity is therefore insufficient for precision photonic, quantum, or optoelectronic devices. This motivates feedback not only on position, but on the local material state itself, exactly the role that multidimensional holographic and polarisation-resolved diagnostics are designed to fill.

The resulting properties may vary laterally, axially, and through the depth of the substrate, so the fabricated structure should be regarded as an embedded heterostructure rather than as a simple surface relief or binary exposure pattern. Consequently, the 3D challenge in femtosecond lithography is not only to track the surface, but also to suppress focus drift or compensate substrate curvature. It is to monitor and control the spatial distribution of dissimilar material states inside a volume. A discriminating measurement strategy is therefore required: one that can separate geometrical displacement from changes in refractive index, absorption, scattering, birefringence, crystallinity, conductivity, or phase composition. This motivates the use of multidimensional optical diagnostics, including holographic reconstruction, polarisation-resolved imaging, interferometric depth sensing,

© 2026 by the author(s). Distributed under a Creative Commons CC BY license.

Preprints.org (www.preprints.org) | NOT PEER-REVIEWED | Posted: 15 May 2026 doi:10.20944/preprints202605.1037.v1

and high-speed transient monitoring, as components of an adaptive lithography loop rather than as post-process inspection tools.

5. Computational Imaging-Based Adaptive Lithography

Among the computational imaging modalities suited to in-process monitoring of femtosecond direct write, another solution to be considered is the four-polarisation (4-pol.) method [111,112]. It is characterised by acquiring images at four sequential linear polarisation orientations, the method reconstructs edge contrast and feature orientation at spatial frequencies beyond the conventional diffraction limit, in both transmission and reflection geometries. This super-resolution edge sensitivity makes 4-pol. imaging a candidate for detecting sub-voxel material transitions, such as crystallinity change or refractive index modification, without requiring physical contact with the sample. These virtues can be harnessed in monitoring and feedback, enabling adaptive correction not only of focus position but of the written property distribution itself.

The future of large-area and 3D nanofabrication is increasingly shaped by the convergence of lithography with computational imaging. While conventional lithography focuses on controlled material exposure, computational imaging provides quantitative reconstruction of optical fields and material responses, enabling adaptive, feedback-driven fabrication. In this context, holography represents a natural bridge between imaging and fabrication, as it encodes the full optical wavefront and enables reconstruction of 3D information relevant to both pattern formation and process control.

Lithography and holography share a common physical basis in diffraction and interference. Optical lithography defines structures by spatially controlling the exposure of a resist, whereas holography reconstructs the amplitude and phase of optical fields that generate these exposure distributions. This shared wave-optical foundation enables holography to extend lithographic capabilities beyond static pattern definition toward dynamic control of exposure, alignment, and material interaction.

A key emerging direction is the integration of computational wavefront reconstruction into fabrication workflows [113–117]. Rather than relying solely on pre-defined exposure conditions, computational imaging enables post-acquisition analysis of the optical field and fabricated structure, allowing adaptive correction of aberrations, alignment errors, and process variations. Such capability is particularly relevant for large-area direct write lithography, where stitching errors, focus drift, and surface non-uniformity limit pattern fidelity.

Understanding the underlying laser–material interaction during femtosecond fabrication is essential for achieving precise and reproducible pattern formation, particularly in large-area and multi-scale lithography. The interaction of ultrashort laser pulses with matter produces highly transient processes, including plasma formation, material ejection, debris generation, and bubble dynamics in surrounding media. These phenomena directly reflect the local energy deposition and interaction regime and therefore provide valuable diagnostic information for process optimisation.

A conceptual framework for real-time monitoring and feedback control of femtosecond fabrication is illustrated in Figure 4. During laser exposure, transient signatures such as debris ejection and bubble formation are monitored using complementary imaging modalities. Fresnel holography enables depth-resolved reconstruction of the interaction region, allowing volumetric characterisation of the evolving structure and transient features at multiple axial positions. In parallel, high-speed imaging captures time-resolved dynamics of the laser–matter interaction on microsecond time scales, providing direct observation of energy transfer processes and material response [118,119].

© 2026 by the author(s). Distributed under a Creative Commons CC BY license.

Preprints.org (www.preprints.org) | NOT PEER-REVIEWED | Posted: 15 May 2026
doi:10.20944/preprints202605.1037.v1

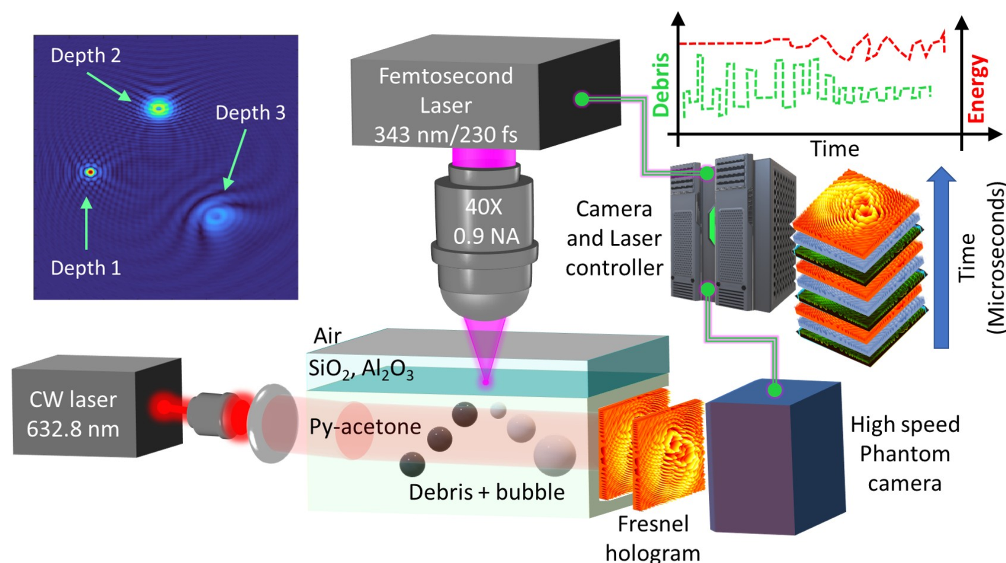

Figure 4. Conceptual scheme of real-time monitoring and feedback control in femtosecond laser fabrication based on characterisation of laser–material interaction dynamics. The actual fabrication without such monitoring was reported in ref. [120].

The spatio-temporal evolution of debris and bubble formation provides insight into local fabrication conditions, including energy deposition, ablation efficiency, and material modification mechanisms. By analysing these interaction signatures in real time, it becomes possible to identify deviations from desired processing regimes and adjust exposure parameters accordingly. Such process-aware monitoring enables adaptive control of laser writing conditions, including pulse energy, focusing conditions, and scanning parameters.

The integration of holographic imaging and high-speed characterisation establishes a computational imaging framework for feedback-controlled fabrication. In this approach, the measured interaction response is processed to infer fabrication conditions and dynamically optimise the writing process. This closed-loop strategy reduces reliance on post-process inspection and provides a pathway toward robust, adaptive, and stitch-less lithographic patterning, particularly for large-area and 3D fabrication.

Beyond sensing and feedback, holography enables a parallel mode of 3D patterning that is inherently stitch-free. Spatial light modulators (SLMs) acting as programmable phase masks can split a single femtosecond beam into hundreds or thousands of independently addressed focal spots, each writing a voxel simultaneously [121]. Digital holography-based two-photon lithography platforms have demonstrated 90 nm resolution with up to 2,000 individually programmable foci and fabrication rates exceeding 2×10^6 voxels/s [121]. At a larger scale, metalens-generated focal spot arrays comprising more than 120,000 cooperative foci across a 12 cm^2 aperture and achieved throughputs exceeding 10^8 voxels/s with sub-micrometre resolution and no stitching discontinuities with an SLM [122]. In this parallel holographic modality, stitching is eliminated not by minimising field-boundary errors but by writing the entire pattern simultaneously within the holographically defined exposure volume. The convergence of such holographic writing capability with the holographic sensing framework defines the full scope of multi-dimensional holography in lithography: exposure, alignment, and real-time process feedback all operating within the same wave-optical framework.

More broadly, real-time characterisation of laser–material interaction represents a transition from open-loop exposure toward interaction-informed fabrication, where process dynamics guide pattern formation. Such approaches are expected to play an increasingly important role in next-generation nanofabrication systems that require high precision, scalability, and multidimensional control.

© 2026 by the author(s). Distributed under a Creative Commons CC BY license.

Preprints.org (www.preprints.org) | NOT PEER-REVIEWED | Posted: 15 May 2026 doi:10.20944/preprints202605.1037.v1

6. Conclusions and Outlook

For applications driven by o-Moore's scaling and enabled by sequential direct write fabrication, the next stage of femtosecond lithography will be characterised by metrics far beyond simple feature size reduction. After approximately 25 years of rapid development in ultrashort-pulse sources, beam delivery, and laser-matter processing, the critical technological directions are now stitch-free writing, multi-beam parallelisation, adaptive beam control, and real-time correction of the writing volume. These requirements arise because direct laser writing is no longer simply a method for drawing geometrical patterns. In many material systems, the written voxel is a local material state whose properties may include refractive index, birefringence, crystallinity, conductivity, oxidation state, defect density, chemical composition, or ferroelectric order. The central hypothesis advanced here is that future femtosecond lithography must treat each voxel as a multi-property object, rather than a binary, exposed or unexposed volume. Stitch-free fabrication is consequently not only a positioning problem; it is a state-continuity problem in which adjacent voxels must preserve the intended optical, electrical, structural, and chemical properties across large areas, curved substrates, heterogeneous stacks, and buried 3D architectures.

This hypothesis strengthens the "Better Before Cheaper" argument. Femtosecond direct laser writing should not be judged only against projection lithography by throughput or cost per unit area, where sequential writing is intrinsically disadvantaged. Its near-term value lies in providing fabrication capabilities that parallel lithography cannot yet deliver: programmable 3D access, local material transformation, compatibility with heterogeneous substrates, rapid design iteration, and adaptive correction at the level of individual features or voxels. In this sense, the role of direct writing is to deliver better functionality before cheaper replication becomes relevant. Once a geometry, process window, or multi-property voxel state has been validated, selected parts of the process may be transferred to higher-throughput methods such as imprinting, projection exposure, or hybrid batch fabrication. However, the discovery, optimisation, and early deployment of complex 3D photonic, optoelectronic, quantum, microfluidic, and packaging architectures will continue to require the flexibility and local controllability of femtosecond direct writing. Development of 3D lithography is expected to have similarity with 3D printing, where the unique advantage value is in complexity and a minimised number of steps (hence net-shape) required for the final product, rather than relying on mass production to deliver a competitive price for the item (Figure 5). As Professor Jean-Marie Lehn (Nobel Prize in Chemistry, 1987) highlighted in his plenary talk at Imagine Nano 2015 in Bilbao, the future of nanotechnology lies in the complexity of developed solutions rather than solely on the pursuit of ever-finer resolution [123]; much like the brain, which operates on a micron scale rather than purely on a nanoscale.

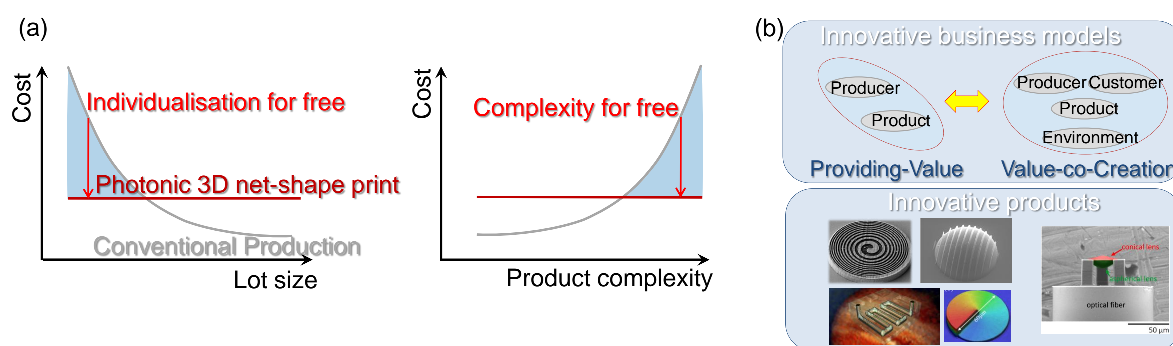

Figure 5. How 3D direct net-shape write prototyping can become industrially competitive in Industry 4.0. (a) Cost dependence on volume and complexity. (b) New 3D net-shape printing innovations in business and products (the model applied for Selective Laser Etching (SLE) at the Fraunhofer Institute for Laser Technology; courtesy of Dr. L. Gottmann).

The future direction is therefore a transition from open-loop exposure to close-loop, interaction-informed state lithography. Computational imaging, multidimensional holography, polarisation-

© 2026 by the author(s). Distributed under a Creative Commons CC BY license.

Preprints.org (www.preprints.org) | NOT PEER-REVIEWED | Posted: 15 May 2026 doi:10.20944/preprints202605.1037.v1

resolved imaging, interferometric focus tracking, optical coherent tomography (OCT)-like depth sensing, plasma-emission diagnostics, and high-speed transient imaging should be integrated not as auxiliary inspection tools, but as components of the fabrication loop. Their task is to estimate the evolving voxel state and update pulse energy, scan speed, focus position, wavefront, polarisation, repetition rate, hatch spacing, and beam multiplexing in real time. To make this transition quantitative, future studies should report complete dose-response maps including pulse energy, average power, fluence, peak intensity, repetition rate, scan speed, pulse overlap, numerical aperture, depth, and accumulated pulse number. Threshold behaviour should be presented using normalised or logarithmic dose coordinates where appropriate, while manufacturing residuals such as line width error, edge placement error, refractive-index variation, loss, birefringence, conductivity, crystallinity, and defect density should also be reported on linear scales. The industrial integration of maskless 3D lithography will depend not merely on multi-beam or stitch-free writing, but on calibrated metrology that links in-situ optical observables to ex-situ material and device performance. This is the route by which femtosecond lithography can remain "better" at the stage where new architectures are invented, and eventually become "cheaper" when those architectures are stabilised and scaled.

Acknowledgments: D.G. was supported by ArtPM project from the Research Council of Lithuania (LMTLT), agreement No. S-MIP-24-10. S.J. acknowledges support via ARC DP240103231 grant. Discussions of nanotechnology trends with Gediminas Gervinskas are acknowledged. We are grateful to Jimmy Wales for his continuous support.

Conflicts of Interest: The authors declare no conflicts of interest.

References

1. Moore, G.E. Cramming More Components onto Integrated Circuits. *Electronics* **1965**, *38*, 114–117.
2. Mack, C.A. Fifty Years of Moore's Law. *IEEE Transactions on Semiconductor Manufacturing* **2011**, *24*, 202–207. https://doi.org/10.1109/TSM.2010.2096437.
3. Lundstrom, M.S.; Alam, M.A. Moore's Law: The Journey Ahead. *Science* **2022**, *378*, 722–723. https://doi.org/10.1126/science.ade2191.
4. Han, M.; Smith, D.; Ng, S.H.; Anand, V.; Katkus, T.; Juodkazis, S. Ultra-Short-Pulse Lasers—Materials—Applications. *Engineering Proceedings* **2021**, *11*. https://doi.org/10.3390/ASEC2021-11143.
5. Mourou, G.A.; Tajima, T.; Bulanov, S.V. Optics in the relativistic regime. *Reviews of Modern Physics* **2006**, *78*, 309–371. https://doi.org/10.1103/RevModPhys.78.309.
6. Reid, D.T.; Heyl, C.M.; Thomson, R.R.; Trebino, R.; Steinmeyer, G.; Fielding, H.H.; Holzwarth, R.; Zhang, Z.; Del'Haye, P.; Südmeyer, T.; et al. Roadmap on ultrafast optics. *Journal of Optics (United Kingdom)* **2016**, *18*. https://doi.org/10.1088/2040-8978/18/9/093006.
7. Ong, J.F.; Teo, W.R.; Moritaka, T.; Takabe, H. Radiation reaction in the interaction of ultraintense laser with matter and gamma ray source. *Physics of Plasmas* **2016**, *23*. https://doi.org/10.1063/1.4952626.
8. Wang, Y.; Tomilov, S.; Saraceno, C.J. High-power modelocked thin-disk oscillators as potential technology for high-rate material processing. *Advanced Optical Technologies* **2021**, *10*, 247–261. https://doi.org/10.1515/aot-2021-0045.
9. Herkommer, C.; Krötz, P.; Jung, R.; Klingebiel, S.; Wandt, C.; Bessing, R.; Walch, P.; Produit, T.; Michel, K.; Bauer, D.; et al. Ultrafast thin-disk multipass amplifier with 720 mJ operating at kilohertz repetition rate for applications in atmospheric research. *Opt. Express* **2020**, *28*, 30164–30173. https://doi.org/10.1364/OE.404185.
10. Giesen, A.; Hügel, H.; Voss, A.; Wittig, K.; Brauch, U.; Opower, H. Scalable concept for diode-pumped high-power solid-state lasers. *Applied Physics B* **1994**, *58*, 365–372.
11. Saraceno, C.J.; Sutter, D.; Metzger, T.; Ahmed, M.A. The amazing progress of high-power ultrafast thin-disk lasers. *Journal of the European Optical Society-Rapid Publications* **2019**, *15*, 15.
12. Russbueldt, P.; Mans, T.; Weitenberg, J.; Hoffmann, H.D.; Poprawe, R. Compact Diode-Pumped 11 kW Yb:YAG Innoslab Femtosecond Amplifier. *Optics letters* **2010**, *35*, 4169–4171. https://doi.org/10.1364/OL.35.004169.

© 2026 by the author(s). Distributed under a Creative Commons CC BY license.

Preprints.org (www.preprints.org) | NOT PEER-REVIEWED | Posted: 15 May 2026 doi:10.20944/preprints202605.1037.v1

13. Heckl, O.H.; Kleinbauer, J.; Bauer, D.; Weiler, S.; Metzger, T.; Sutter, D.H. Ultrafast Thin-Disk Lasers. In *Ultrashort Pulse Laser Technology*; Nolte, S.; Schrempel, F.; Dausinger, F., Eds.; Springer International Publishing: Cham, 2016; Vol. 195, pp. 93–115. https://doi.org/10.1007/978-3-319-17659-8_5.
14. Wang, B.; Peng, R.; Wang, X.; Yang, Y.; Wang, E.; Xin, Z.; Sun, Y.; Li, C.; Wu, Y.; Wei, J.; et al. Ultrafast, Kinetically Limited, Ambient Synthesis of Vanadium Dioxides through Laser Direct Writing on Ultrathin Chalcogenide Matrix. *ACS Nano* **2021**, *15*, 10502–10513. https://doi.org/10.1021/acsnano.1c03050.
15. Malinauskas, M.; Žukauskas, A.; Hasegawa, S.; Hayasaki, Y.; Mizeikis, V.; Buividas, R.; Juodkazis, S. Ultrafast Laser Processing of Materials: From Science to Industry. *Light: Science & Applications* **2016**, *5*, e16133–e16133. https://doi.org/10.1038/lsa.2016.133.
16. Kerse, C.; Kalaycıoğlu, H.; Elahi, P.; Çetin, B.; Kesim, D.K.; Akçaalan, Ö.; Yavaş, S.; Aşık, M.D.; Öktem, B.; Hoogland, H.; et al. Ablation-Cooled Material Removal with Ultrafast Bursts of Pulses. *Nature* **2016**, *537*, 84–88. https://doi.org/10.1038/nature18619.
17. Arakawa, Y. Academic Roadmap. https://www.jsap.or.jp/english/activities/academic-roadmap, 2013.
18. Raynor, M.; Ahmed, M. *The Three Rules: How Exceptional Companies Think*; Penguin Publishing Group, 2013.
19. Mauboussin, M.J.; Callahan, D. Measuring the Moat: Assessing the Magnitude and Sustainability of Value Creation. Consilient observer, Morgan Stanley Investment Management, Counterpoint Global, 2024.
20. Glezer, E.N.; Milosavljevic, M.; Huang, L.; Finlay, R.J.; Her, T.H.; Callan, J.P.; Mazur, E. Three-Dimensional Optical Storage inside Transparent Materials. *Optics Letters* **1996**, *21*, 2023. https://doi.org/10.1364/OL.21.002023.
21. Watanabe, M.; Sun, H.; Juodkazis, S.; Takahashi, T.; Matsuo, S.; Suzuki, Y.; Nishii, J.; Misawa, H. Three-Dimensional Optical Data Storage in Vitreous Silica. *Japanese Journal of Applied Physics* **1998**, *37*, L1527. https://doi.org/10.1143/JJAP.37.L1527.
22. Nakano, M.; Kooriya, T.; Kuragaito, T.; Egami, C.; Kawata, Y.; Tsuchimori, M.; Watanabe, O. Three-Dimensional Patterned Media for Ultrahigh-Density Optical Memory. *Applied Physics Letters* **2004**, *85*, 176–178. https://doi.org/10.1063/1.1771800.
23. Lin, S.; Lin, H.; Ma, C.; Cheng, Y.; Ye, S.; Lin, F.; Li, R.; Xu, J.; Wang, Y. High-Security-Level Multi-Dimensional Optical Storage Medium: Nanostructured Glass Embedded with LiGa5O8: Mn2+ with Photostimulated Luminescence. *Light: Science & Applications* **2020**, *9*, 22. https://doi.org/10.1038/s41377-020-0258-3.
24. IEEE International Roadmap for Devices and Systems. IEEE International Roadmap for Devices and Systems: Lithography and Patterning. Institute of Electrical and Electronics Engineers, 2024. https://irds.ieee.org/images/files/pdf/2024/2024IRDS_LITHO.pdf.
25. Maksimovic, J.; Hu, J.; Ng, S.H.; Katkus, T.; Seniutinas, G.; Rivera, T.P.; Stuiber, M.; Nishijima, Y.; John, S.; Juodkazis, S. Beyond Lambertian light trapping for large-area silicon solar cells: fabrication methods. *Opto-Electronic Advances* **2022**, *5*, 210086–1–210086–12. https://doi.org/10.29026/oea.2022.210086.
26. Gross, S.; Withford, M.J. Ultrafast-laser-inscribed 3D Integrated Photonics: Challenges and Emerging Applications. *Nanophotonics* **2015**, *4*, 332–352. https://doi.org/10.1515/nanoph-2015-0020.
27. Sima, F.; Xu, J.; Wu, D.; Sugioka, K. Ultrafast Laser Fabrication of Functional Biochips: New Avenues for Exploring 3D Micro- and Nano-Environments. *Micromachines* **2017**, *8*, 40. https://doi.org/10.3390/mi8020040.
28. Berzinš, J.; Indrišiūnas, S.; Van Erve, K.; Nagarajan, A.; Fasold, S.; Steinert, M.; Gerini, G.; Gečys, P.; Pertsch, T.; Bäumer, S.M.B.; et al. Direct and High-Throughput Fabrication of Mie-Resonant Metasurfaces *via* Single-Pulse Laser Interference. *ACS Nano* **2020**, *14*, 6138–6149. https://doi.org/10.1021/acsnano.0c01993.
29. Orazi, L.; Romoli, L.; Schmidt, M.; Li, L. Ultrafast Laser Manufacturing: From Physics to Industrial Applications. *CIRP Annals* **2021**, *70*, 543–566. https://doi.org/10.1016/j.cirp.2021.05.007.
30. Beisenova, A.; Adi, W.; Wu, W.; Biswas, S.K.; Rosas, S.; Stamenic, B.; John, D.D.; Yesilkoy, F. Wafer-Scale All-Dielectric Quasi-BIC Metasurfaces: Bridging High-Throughput Deep-UV Lithography with Nanophotonic Applications. *Nano Letters* **2026**, *26*, 2059–2067. https://doi.org/10.1021/acs.nanolett.5c05226.
31. Li, D.W.; Zhou, Y.S.; Huang, X.; Jiang, L.; Silvain, J.F.; Lu, Y.F. In situ imaging and control of layer-by-layer femtosecond laser thinning of graphene. *Nanoscale* **2015**, *7*, 3651–3659. https://doi.org/10.1039/C4NR07078J.
32. Qin, F.; Liu, B.; Zhu, L.; Lei, J.; Fang, W.; Hu, D.; Zhu, Y.; Ma, W.; Wang, B.; Shi, T.; et al. π-Phase Modulated Monolayer Supercritical Lens. *Nat Commun* **2021**, *12*, 32. https://doi.org/10.1038/s41467-020-20278-x.
33. Zhang, W.; Shi, Z.; Chen, C.; Yang, X.; Yang, L.; Zeng, Z.; Zhang, B.; Liu, Q. Super-resolution GaAs nano-structures fabricated by laser direct writing. *Materials Science in Semiconductor Processing* **2018**, *84*, 119–123. https://doi.org/10.1016/j.mssp.2018.05.016.

© 2026 by the author(s). Distributed under a Creative Commons CC BY license.

Preprints.org (www.preprints.org) | NOT PEER-REVIEWED | Posted: 15 May 2026 doi:10.20944/preprints202605.1037.v1

34. Enrico, A.; Hartwig, O.; Dominik, N.; Quellmalz, A.; Gylfason, K.B.; Duesberg, G.S.; Niklaus, F.; Stemme, G. Ultrafast and Resist-Free Nanopatterning of 2D Materials by Femtosecond Laser Irradiation. *ACS Nano* **2023**, *17*, 8041–8052. https://doi.org/10.1021/acsnano.2c09501.
35. Zhu, H.; Wu, B.; Gao, M.; Ren, F.; Qin, W.; Juodkazis, S.; Chen, F. Femtosecond Laser Direct-Write Plasmonic Nanolithography in Dielectrics. *Small Science* **2022**, *2*, 2200038. https://doi.org/10.1002/smsc.202200038.
36. Sharma, E.; Rathi, R.; Misharwal, J.; Sinhmar, B.; Kumari, S.; Dalal, J.; Kumar, A. Evolution in Lithography Techniques: Microlithography to Nanolithography. *Nanomaterials* **2022**, *12*. https://doi.org/10.3390/nano12162754.
37. Zhang, W.; Han, L.H.; Chen, S. Integrated Two-Photon Polymerization With Nanoimprinting for Direct Digital Nanomanufacturing. *Journal of Manufacturing Science and Engineering* **2010**, *132*. https://doi.org/10.1115/1.4001661.
38. Saive, R.; Bukowsky, C.R.; Atwater, H.A. Three-Dimensional Nanoimprint Lithography Using Two-Photon Lithography Master Samples, 2017. https://doi.org/10.48550/ARXIV.1702.04012.
39. Perak, S.; Kopp, S.; Jonaityte, V.; Bonora, M.; Muehlberger, M.; Moscato, F.; Lunzer, M. Two-photon polymerization lithography as a mastering tool for nanoimprint lithography. In Proceedings of the 40th European Mask and Lithography Conference (EMLC 2025); Finders, J.; Stolberg, I., Eds. International Society for Optics and Photonics, SPIE, 2025, Vol. 13787, p. 137870R. https://doi.org/10.1117/12.3065994.
40. Brenner, P.; Bar-On, O.; Siegle, T.; Leonhard, T.; Gvishi, R.; Eschenbaum, C.; Kalt, H.; Scheuer, J.; Lemmer, U. 3D whispering-gallery-mode microlasers by direct laser writing and subsequent soft nanoimprint lithography. *Appl. Opt.* **2017**, *56*, 3703–3708. https://doi.org/10.1364/AO.56.003703.
41. Bar-On, O.; Brenner, P.; Siegle, T.; Gvishi, R.; Kalt, H.; Lemmer, U.; Scheuer, J. High Quality 3D Photonics using Nano Imprint Lithography of Fast Sol-gel Materials. *Scientific Reports* **2018**, *8*. https://doi.org/10.1038/s41598-018-26261-3.
42. Seidel, A.; Ohrt, C.; Passinger, S.; Reinhardt, C.; Kiyan, R.; Chichkov, B.N. Nanoimprinting of dielectric loaded surface-plasmon-polariton waveguides using masters fabricated by 2-photon polymerization technique. *J. Opt. Soc. Am. B* **2009**, *26*, 810–812. https://doi.org/10.1364/JOSAB.26.000810.
43. Lightman, S.; Gvishi, R.; Hurvitz, G.; Arie, A. Comparative analysis of direct laser writing and nanoimprint lithography for fabrication of optical phase elements. *Applied Optics* **2016**, *55*, 9724. https://doi.org/10.1364/AO.55.009724.
44. Xiao, T.P.; Cifci, O.S.; Bhargava, S.; Chen, H.; Gissibl, T.; Zhou, W.; Giessen, H.; Toussaint, K.C.; Yablonovitch, E.; Braun, P.V. Diffractive Spectral-Splitting Optical Element Designed by Adjoint-Based Electromagnetic Optimization and Fabricated by Femtosecond 3D Direct Laser Writing. *ACS Photonics* **2016**, *3*, 886–894. https://doi.org/10.1021/acsphotonics.6b00066.
45. Murphy, T.E.; Mondol, M.K.; Smith, H.I. Characterization of field stitching in electron-beam lithography using moiré metrology. *Journal of Vacuum Science & Technology B: Microelectronics and Nanometer Structures* **2000**, *18*, 3287–3291. https://doi.org/10.1116/1.1313573.
46. Thoms, S.; Macintyre, D.S. Tilt-corrected stitching for electron beam lithography. *Microelectronic Engineering* **2007**, *84*, 793–796. https://doi.org/10.1016/j.mee.2007.01.127.
47. Miyoshi, H.; Taniguchi, J. Fabrication of a high-resolution mask by using variable-shaped electron beam lithography with a non-chemically amplified resist and a post-exposure bake. *Microelectronic Engineering* **2015**, *143*, 48–54. https://doi.org/10.1016/j.mee.2015.03.026.
48. Patsis, G.P.; Tsikrikas, N.; Raptis, I.; Glezos, N. Electron-beam lithography simulation for the fabrication of EUV masks. *Microelectronic Engineering* **2006**, *83*, 1148–1151. https://doi.org/10.1016/j.mee.2006.01.040.
49. George, S.M.; Naulleau, P.; Brainard, R.L.; et al. Extreme ultraviolet mask surface cleaning effects on lithography process performance. *Journal of Vacuum Science & Technology B* **2010**, *28*, C6E31. https://doi.org/10.1116/1.3501344.
50. Maibohm, C.; Ristok, S.; Carpinteiro, A.; et al. Multi-beam two-photon polymerization for fast large area 3D periodic structure fabrication. *Scientific Reports* **2020**, *10*, 8741. https://doi.org/10.1038/s41598-020-64955-9.
51. Khodadad, I.; Nelson-Fitzpatrick, N.; Burcham, K.; Hajian, A.; Saini, S.S. Electron beam lithography using fixed beam moving stage. *Journal of Vacuum Science & Technology B* **2017**, *35*, 051601. https://doi.org/10.1116/1.4997018.
52. Goodberlet, J.G.; Hastings, J.T.; Smith, H.I. Performance of the Raith 150 electron-beam lithography system. *Journal of Vacuum Science & Technology B* **2001**, *19*, 2499–2503. https://doi.org/10.1116/1.1414018.

© 2026 by the author(s). Distributed under a Creative Commons CC BY license.

Preprints.org (www.preprints.org) | NOT PEER-REVIEWED | Posted: 15 May 2026 doi:10.20944/preprints202605.1037.v1

53. Stenkamp, D.; Kienzle, O.; Orchowski, A.; et al. Progress on the realization of the electron column modules for SCALPEL high-throughput/alpha electron projection lithography tools. *Microelectronic Engineering* **2001**, *57*, 137–143. https://doi.org/10.1016/S0167-9317(01)00505-6.
54. Dehaeck, S.; Scheid, B.; Lambert, P. Adaptive stitching for meso-scale printing with two-photon lithography. *Additive Manufacturing* **2018**, *21*, 589–597. https://doi.org/10.1016/j.addma.2018.03.026.
55. Jonušauskas, L.; Baravykas, T.; Andrijec, D.; Gadišauskas, T.; Purlys, V. Stitchless support-free 3D printing of free-form micromechanical structures with feature size on-demand. *Scientific Reports* **2019**, *9*, 17533. https://doi.org/10.1038/s41598-019-54024-1.
56. Ren, M.; Lu, W.; Shao, Q.; et al. Aberration-free large-area stitch-free 3D nano-printing based on binary holography. *Optics Express* **2021**, *29*, 44250–44263. https://doi.org/10.1364/OE.446503.
57. Jonušauskas, L.; Gailevičius, D.; Rekštytė, S.; Baldacchini, T.; Juodkazis, S.; Malinauskas, M. Mesoscale laser 3D printing. *Optics Express* **2019**, *27*, 15205–15221. https://doi.org/10.1364/OE.27.015205.
58. Adão, R.M.R.; Alves, T.L.; Maibohm, C.; Romeira, B.; Nieder, J.B. Two-photon polymerization simulation and fabrication of 3D microprinted suspended waveguides for on-chip optical interconnects. *Optics Express* **2022**, *30*, 9623–9642. https://doi.org/10.1364/OE.449641.
59. Fujishiro, Y.; Furukawa, T.; Maruo, S. Simple autofocusing method by image processing using transmission images for large-scale two-photon lithography. *Optics Express* **2020**, *28*, 12342–12351. https://doi.org/10.1364/OE.390486.
60. Chini, S.F.; Amirfazli, A.; et al. Understanding pattern collapse in photolithography. *Langmuir* **2010**, *26*, 13707–13715. https://doi.org/10.1021/la1033524.
61. Kalaiselvi, S.; Narayanan, S.L.; Rangarajan, S. Optimization of corner compensations in wet etching of silicon for a MEMS Z-axis accelerometer. *Microelectronic Engineering* **2022**, *258*, 111771. https://doi.org/10.1016/j.mee.2022.111771.
62. Zhang, Y.; Hou, Z.; Ning, X.; Yang, Z. Effects of mask material on lateral undercut of silicon dry etching. *Micromachines* **2023**, *14*, 306. https://doi.org/10.3390/mi14020306.
63. Morello, G.; Quaglio, M.; Meneghini, M.; et al. Reactive ion etching induced damage evaluation for optoelectronic device fabrication. *Journal of Vacuum Science & Technology B* **2006**, *24*, 756–760. https://doi.org/10.1116/1.2185591.
64. Ko, K.K.; Pang, S.W. Plasma Passivation of Etch-Induced Surface Damage on GaAs. *Journal of Vacuum Science & Technology B: Microelectronics and Nanometer Structures Processing, Measurement, and Phenomena* **1995**, *13*, 2376–2380. https://doi.org/10.1116/1.588077.
65. Maksimovic, J.; Mu, H.; Smith, D.; Katkus, T.; Vaičiulis, M.; Aleksiejūnas, R.; Seniutinas, G.; Ng, S.H.; Juodkazis, S. Laser-Patterned Alumina Mask and Mask-Less Dry Etch of Si for Light Trapping with Photonic Crystal Structures. *Micromachines* **2023**, *14*, 550. https://doi.org/10.3390/mi14030550.
66. Katkus, T.; Ng, S.H.; Mu, H.; Le, N.H.A.; et al. Bessel-Beam Direct Write of the Etch Mask in a Nano-Film of Alumina for High-Efficiency Si Solar Cells. *Advanced Engineering Materials* **2024**, *26*, 2400711. https://doi.org/10.1002/adem.202400711.
67. Maksimovic, J.; Hu, J.; Ng, S.H.; Katkus, T.; Seniutinas, G.; Rivera, T.P.; Stuiber, M.; Nishijima, Y.; John, S.; Juodkazis, S. Beyond Lambertian light trapping for large-area silicon solar cells: fabrication methods. *Opto-Electronic Advances* **2022**, *5*, 210086. https://doi.org/10.29026/oea.2022.210086.
68. Rienäcker, M.; Römer, U.; Krügener, J.; Maksimovic, J.; Katkus, T.; Stonytė, D.; et al. Integration of Laser-Patterned Photonic Crystals in Si Solar Cells. *Advanced Optical Materials* **2025**, *13*, e01781. https://doi.org/10.1002/adom.202501781.
69. Bhattacharya, S.; Baydoun, M.; Lin, S.Y.; John, S. Towards 30% power conversion efficiency in thinner silicon photovoltaics using nanophotonic light-trapping. *Physical Review Applied* **2019**, *11*, 014005. https://doi.org/10.1103/PhysRevApplied.11.014005.
70. Maury, P.; Quemper, J.M.; Pocas, S.; Van Vliet, D.; Noordam, N.; ten Berge, P.; Best, K. Sub-micron imaging on high-topography wafers using spray coating and projection lithography. *Microelectronic Engineering* **2010**, *87*, 904–906. https://doi.org/10.1016/j.mee.2009.11.083.
71. Mansuripur, M. Analysis of astigmatic focusing and push–pull tracking error signals in magnetooptical disk systems. *Appl. Opt.* **1987**, *26*, 3981–3986. https://doi.org/10.1364/AO.26.003981.
72. Bernacki, B.E.; Mansuripur, M. Causes of focus-error feedthrough in optical-disk systems: astigmatic and obscuration methods. *Appl. Opt.* **1994**, *33*, 735–743. https://doi.org/10.1364/AO.33.000735.

© 2026 by the author(s). Distributed under a Creative Commons CC BY license.

Preprints.org (www.preprints.org) | NOT PEER-REVIEWED | Posted: 15 May 2026 doi:10.20944/preprints202605.1037.v1

73. Hsu, W.Y.; Lee, C.S.; Chen, P.J.; Chen, N.T.; Chen, F.Z.; Yu, Z.R.; Kuo, C.H.; Hwang, C.H. Development of the fast astigmatic auto-focus microscope system. *Measurement Science and Technology* **2009**, *20*, 045902. https://doi.org/10.1088/0957-0233/20/4/045902.
74. Rahmani, A.; Cox, T.; Achary, A.T.A.; Ponjavic, A. Astigmatism-based active focus stabilisation with universal objective lens compatibility, extended operating range and nanometer precision. *Optics Express* **2024**, *32*, 13331. https://doi.org/10.1364/OE.520845.
75. Vo, Q.; Fang, F.; Zhang, X.; Zhu, L. Reducing the residual focus error signal in optical pickup head astigmatism displacement systems using the signal conditioning method. *Appl. Opt.* **2018**, *57*, 9972–9980. https://doi.org/10.1364/AO.57.009972.
76. hoon Yoo, J.; woo Lee, C.; ho Shin, D.; Bartlett, C.; lu Cheong, K.; Erwin, J.K.; Mansuripur, M. Investigation of certain diffraction effects in an optical disk. *Appl. Opt.* **1997**, *36*, 9287–9295. https://doi.org/10.1364/AO.36.009287.
77. Liu, C.H.; Yeh, S.C.; Huang, H.L. Thickness measurement system for transparent plates using dual digital versatile disc (DVD) pickups. *Appl. Opt.* **2010**, *49*, 637–643. https://doi.org/10.1364/AO.49.000637.
78. Liao, H.S.; Cheng, S.H.; Hwu, E.T. Method for Film Thickness Mapping with an Astigmatic Optical Profilometer. *Sensors* **2022**, *22*. https://doi.org/10.3390/s22082865.
79. Chen, L.C. Full-field chromatic confocal surface profilometry employing digital micromirror device correspondence for minimizing lateral cross talks. *Optical Engineering* **2012**, *51*, 081507. https://doi.org/10.1117/1.oe.51.8.081507.
80. Chen, L.C.; Nguyen, D.T.; Chang, Y.W. Precise optical surface profilometry using innovative chromatic differential confocal microscopy. *Opt. Lett.* **2016**, *41*, 5660–5663. https://doi.org/10.1364/OL.41.005660.
81. Liu, T.; Hong, Y.; Wu, J.; Zhu, W.; Ju, B. A New Method for Measuring Multilayer Thickness Using a Chromatic Confocal Sensor. *Nanomanufacturing and Metrology* **2024**, *7*. https://doi.org/10.1007/s41871-024-00241-w.
82. Petráň, M.; Hadravský, M.; Egger, M.D.; Galambos, R. Tandem-Scanning Reflected-Light Microscope. *J. Opt. Soc. Am.* **1968**, *58*, 661–664. https://doi.org/10.1364/JOSA.58.000661.
83. Davidovits, P.; Egger, M.D. Scanning Laser Microscope for Biological Investigations. *Appl. Opt.* **1971**, *10*, 1615–1619. https://doi.org/10.1364/AO.10.001615.
84. Kimura, S.; Wilson, T. Effect of axial pinhole displacement in confocal microscopes. *Appl. Opt.* **1993**, *32*, 2257–2261. https://doi.org/10.1364/AO.32.002257.
85. Lee, D.R.; Jang, S.; woo Lee, M.; Yoo, H. Compact fiber optic dual-detection confocal displacement sensor. *Appl. Opt.* **2016**, *55*, 7631–7635. https://doi.org/10.1364/AO.55.007631.
86. Nakazawa, K.; Sasaki, T.; Furuta, H.; Kamiya, J.; Sasaki, H.; Kamiya, T.; Hane, K. Confocal laser displacement sensor using a micro-machined varifocal mirror. *Appl. Opt.* **2017**, *56*, 6911–6916. https://doi.org/10.1364/AO.56.006911.
87. Park, J.; Kim, S.W. Active autofocus control using source dithering technique based on fibre-optic confocal principle. *International Journal of Precision Engineering and Manufacturing* **2011**, *12*, 733–736. https://doi.org/10.1007/s12541-011-0095-7.
88. Lee, B.S.; Strand, T.C. Profilometry with a Coherence Scanning Microscope. *Applied Optics* **1990**, *29*, 3784. https://doi.org/10.1364/AO.29.003784.
89. Deck, L.; de Groot, P. High-speed noncontact profiler based on scanning white-light interferometry. *Appl. Opt.* **1994**, *33*, 7334–7338. https://doi.org/10.1364/AO.33.007334.
90. Schmit, J.; Olszak, A. High-Precision Shape Measurement by White-Light Interferometry with Real-Time Scanner Error Correction. *Applied Optics* **2002**, *41*, 5943. https://doi.org/10.1364/AO.41.005943.
91. Flournoy, P.A.; McClure, R.W.; Wyntjes, G. White-Light Interferometric Thickness Gauge. *Applied Optics* **1972**, *11*, 1907. https://doi.org/10.1364/AO.11.001907.
92. Yun, S.H.; Tearney, G.J.; de Boer, J.F.; Iftimia, N.; Bouma, B.E. High-speed optical frequency-domain imaging. *Opt. Express* **2003**, *11*, 2953–2963. https://doi.org/10.1364/OE.11.002953.
93. Leitgeb, R.; Hitzenberger, C.K.; Fercher, A.F. Performance of fourier domain vs. time domain optical coherence tomography. *Opt. Express* **2003**, *11*, 889–894. https://doi.org/10.1364/OE.11.000889.
94. Kino, G.S.; Chim, S.S.C. Mirau correlation microscope. *Appl. Opt.* **1990**, *29*, 3775–3783. https://doi.org/10.1364/AO.29.003775.
95. Pavliček, P.; Halouzka, M.; Duan, Z.; Takeda, M. Spatial coherence profilometry on tilted surfaces. *Appl. Opt.* **2009**, *48*, H40–H47. https://doi.org/10.1364/AO.48.000H40.

© 2026 by the author(s). Distributed under a Creative Commons CC BY license.

Preprints.org (www.preprints.org) | NOT PEER-REVIEWED | Posted: 15 May 2026 doi:10.20944/preprints202605.1037.v1

96. Ustun, T.E.; Iftimia, N.V.; Ferguson, R.D.; Hammer, D.X. Real-time processing for Fourier domain optical coherence tomography using a field programmable gate array. *Review of Scientific Instruments* **2008**, *79*. https://doi.org/10.1063/1.3005996.
97. Watanabe, Y.; Maeno, S.; Aoshima, K.; Hasegawa, H.; Koseki, H. Real-time processing for full-range Fourier-domain optical-coherence tomography with zero-filling interpolation using multiple graphic processing units. *Appl. Opt.* **2010**, *49*, 4756–4762. https://doi.org/10.1364/AO.49.004756.
98. Vishnubhatla, K.; Rao, S.V.; Kumar, R.S.S.; Ferrari, M.; Rao, D.N. Optical studies of two dimensional gratings in fused silica, GE 124, and Foturan™ glasses fabricated using femtosecond laser pulses. *Optics Communications* **2009**, *282*, 4537–4542. https://doi.org/10.1016/j.optcom.2009.08.041.
99. Cerkauskaite, A.; Drevinskas, R.; Solodar, A.; Abdulhalim, I.; Kazansky, P.G. Form-Birefringence in ITO Thin Films Engineered by Ultrafast Laser Nanostructuring. *ACS Photonics* **2017**, *4*, 2944–2951. https://doi.org/10.1021/acsphotonics.7b01082.
100. Lucherini, L.; Navello, V.; Akouissi, O.; Lacour, S.P.; Amstad, E. Direct laser writing of electronically conductive microstructures within soft hydrogel substrates. *Materials Today Bio* **2025**, *34*, 102140. https://doi.org/10.1016/j.mtbio.2025.102140.
101. Garcia-Lechuga, M.; Casquero, N.; Siegel, J.; Solis, J.; Clady, R.; Wang, A.; Utéza, O.; Grojo, D. Amorphization and Ablation of Crystalline Silicon Using Ultrafast Lasers: Dependencies on the Pulse Duration and Irradiation Wavelength. *Laser and Photonics Reviews* **2024**, *2301327*. https://doi.org/10.1002/lpor.202301327.
102. Chen, Y.C.; Griffiths, B.; Weng, L.; Nicley, S.S.; Ishmael, S.N.; Lekhai, Y.; Johnson, S.; Stephen, C.J.; Green, B.L.; Morley, G.W.; et al. Laser writing of individual nitrogen-vacancy defects in diamond with near-unity yield. *Optica* **2019**, *6*, 662. https://doi.org/10.1364/OPTICA.6.000662.
103. Carpentier, M.; Alassani, F.; Cardinal, T.; Canioni, L.; Petit, Y. Femtosecond direct laser writing of an integrated gain medium in the near-IR range in a bismuth containing glass. *Optics Letters* **2025**, *50*, 3273. https://doi.org/10.1364/OL.559043.
104. Calmano, T.; Paschke, A.G.; Siebenmorgen, J.; Fredrich-Thornton, S.T.; Yagi, H.; Petermann, K.; Huber, G. Characterization of an Yb:YAG ceramic waveguide laser, fabricated by the direct femtosecond-laser writing technique. *Applied Physics B* **2011**, *103*, 1–4. https://doi.org/10.1007/s00340-011-4485-4.
105. Maksimovic, J.; Mu, H.; Han, M.; Smith, D.; Katkus, T.; Anand, V.; Nishijima, Y.; Ng, S.H.; Juodkazis, S. Si-Cr Nano-Alloys Fabricated by Direct Femtosecond Laser Writing. *Materials* **2023**, *16*, 1917. https://doi.org/10.3390/ma16051917.
106. Kononenko, T.; Komlenok, M.; Pashinin, V.; Pimenov, S.; Konov, V.; Neff, M.; Romano, V.; Lüthy, W. Femtosecond laser microstructuring in the bulk of diamond. *Diamond and Related Materials* **2009**, *18*, 196–199. https://doi.org/10.1016/j.diamond.2008.07.014.
107. Ashikkalieva, K.; Kononenko, T.; Obraztsova, E.; Zavedeev, E.; Khomich, A.; Ashkinazi, E.; Konov, V. Direct observation of graphenic nanostructures inside femtosecond-laser modified diamond. *Carbon* **2016**, *102*, 383–389. https://doi.org/10.1016/j.carbon.2016.02.044.
108. Sun, X.; Ehrhardt, M.; Lotnyk, A.; Lorenz, P.; Thelander, E.; Gerlach, J.W.; Smausz, T.; Decker, U.; Rauschenbach, B. Crystallization of Ge2Sb2Te5 thin films by nano- and femtosecond single laser pulse irradiation. *Scientific Reports* **2016**, *6*, 28246. https://doi.org/10.1038/srep28246.
109. Zou, T.; Zhao, B.; Xin, W.; Wang, Y.; Wang, B.; Zheng, X.; Xie, H.; Zhang, Z.; Yang, J.; Guo, C.L. High-speed femtosecond laser plasmonic lithography and reduction of graphene oxide for anisotropic photoresponse. *Light: Science and Applications* **2020**, *9*. https://doi.org/10.1038/s41377-020-0311-2.
110. Long, J.; Chen, X.; Mao, T.; Xue, S.; Wang, Y.; Xu, Y.; Pi, W.; Lu, J.; Luo, W.; Xiong, W. Laser Direct Writing of Sol–Gel-Derived Vacancy-Rich Functional Oxide Semiconductors. *ACS Nano* **2023**, *17*, 10033–10040. https://doi.org/10.1021/acsnano.2c12163.
111. Gassner, C.; Vongsvivut, J.; Ryu, M.; Ng, S.H.; Toplak, M.; Anand, V.; Takkalkar, P.; Fac, M.L.; Sims, N.A.; Wood, B.R.; et al. Bridging spectroscopy and advanced molecular orientation analysis with new 4+ angle polarization toolbox in Quasar. *Computers in Biology and Medicine* **2025**, *196*, 110573. https://doi.org/https://doi.org/10.1016/j.compbiomed.2025.110573.
112. Honda, R.; Ryu, M.; Moritake, M.; Balčytis, A.; Mizeikis, V.; Vongsvivut, J.; Tobin, M.J.; Appadoo, D.; Li, J.L.; Ng, S.H.; et al. Infrared Polariscopy Imaging of Linear Polymeric Patterns with a Focal Plane Array. *Nanomaterials* **2019**, *9*. https://doi.org/10.3390/nano9050732.
113. Huang, Z.; Cao, L. Quantitative phase imaging based on holography: trends and new perspectives. *Light: Science & Applications* **2024**, *13*, 145.

© 2026 by the author(s). Distributed under a Creative Commons CC BY license.

Preprints.org (www.preprints.org) | NOT PEER-REVIEWED | Posted: 15 May 2026 doi:10.20944/preprints202605.1037.v1

114. Wang, Z.; Miccio, L.; Coppola, S.; Bianco, V.; Memmolo, P.; Tkachenko, V.; Ferraro, V.; Di Maio, E.; Maffettone, P.L.; Ferraro, P. Digital holography as metrology tool at micro-nanoscale for soft matter. *Light: Advanced Manufacturing* **2022**, *3*, 151–176.
115. Paturzo, M.; Pagliarulo, V.; Bianco, V.; Memmolo, P.; Miccio, L.; Merola, F.; Ferraro, P. Digital Holography, a metrological tool for quantitative analysis: Trends and future applications. *Optics and Lasers in Engineering* **2018**, *104*, 32–47.
116. Kumar, M.; Pensia, L.; Kaur, K.; Kumar, R.; Awatsuji, Y.; Matoba, O. Advances in Optical Metrology: High-bandwidth Digital Holography for Transparent Objects Analysis. In Proceedings of the Photonics. MDPI, 2025, Vol. 12, p. 617.
117. Yang, Y.; Liu, K.; Gao, Y.; Wang, C.; Cao, L. Advancements and challenges in inverse lithography technology: a review of artificial intelligence-based approaches. *Light: Science & Applications* **2025**, *14*, 250.
118. Ng, S.H.; Anand, V.; Katkus, T.; Juodkazis, S. Invasive and Non-Invasive Observation of Occluded Fast Transient Events: Computational Tools. *Photonics* **2021**, *8*, 253. https://doi.org/10.3390/photonics8070253.
119. Anand, V.; Ng, S.H.; Katkus, T.; Juodkazis, S. Spatio-Spectral-Temporal Imaging of Fast Transient Phenomena Using a Random Array of Pinholes. *Advanced Photonics Research* **2021**, *2*, 2000032.
120. Hua, J.G.; Ren, H.; Huang, J.; Luan, M.L.; Chen, Q.D.; Juodkazis, S.; Sun, H.B. Laser-Induced Cavitation-Assisted True 3D Nano-Sculpturing of Hard Materials. *Small* **2023**, *19*, 2207968, [https://onlinelibrary.wiley.com/doi/pdf/10.1002/smll.202207968]. https://doi.org/https://doi.org/10.1002/smll.202207968.
121. Ouyang, W.; Xu, X.; Lu, W.; Zhao, N.; Han, F.; Chen, S.C. Ultrafast 3D Nanofabrication via Digital Holography. *Nature Communications* **2023**, *14*, 1716. https://doi.org/10.1038/s41467-023-37163-y.
122. Gu, S.; Mao, C.; Guell Izard, A.; Sadana, S.; Terrel-Perez, D.; Mettry-Yassa, M.; Choi, W.; Zhou, W.; Yan, H.; Zhou, Z.; et al. 3D Nanolithography with Metalens Arrays and Spatially Adaptive Illumination. *Nature* **2025**, *648*, 591–599. https://doi.org/10.1038/s41586-025-09842-x.
123. Lehn, J.M. The Self-Organization Approach. Imaginenano Plenary Session at ImagineNano 2015, 2015.

Disclaimer/Publisher's Note: The statements, opinions and data contained in all publications are solely those of the individual author(s) and contributor(s) and not of MDPI and/or the editor(s). MDPI and/or the editor(s) disclaim responsibility for any injury to people or property resulting from any ideas, methods, instructions or products referred to in the content.

© 2026 by the author(s). Distributed under a Creative Commons CC BY license.